

Relationships between outgoing longwave radiation and diabatic heating in reanalyses

Kai Zhang¹  · William J. Randel² · Rong Fu^{1,3}

Received: 11 July 2016 / Accepted: 16 December 2016
© Springer-Verlag Berlin Heidelberg 2016

Abstract This study investigates relationships between daily variability in National Oceanographic and Atmospheric Administration (NOAA) outgoing longwave radiation (OLR), as a proxy for deep convection, and the global diabatic heat budget derived from reanalysis data sets. Results are evaluated based on data from ECMWF Reanalysis (ERA-Interim), Japanese 55-year Reanalysis (JRA-55) and Modern-Era Retrospective Analysis for Research and Applications (MERRA2). The diabatic heating is separated into components linked to ‘physics’ (mainly latent heat fluxes), plus longwave (LW) and shortwave (SW) radiative tendencies. Transient variability in deep convection is highly correlated with diabatic heating throughout the troposphere and stratosphere. Correlation patterns and composite analyses show that enhanced deep convection (lower OLR) is linked to amplified heating in the tropical troposphere and in the mid-latitude storm tracks, tied to latent heat release. Enhanced convection is also linked to radiative cooling in the lower stratosphere, due to weaker upwelling LW from lower altitudes. Enhanced transient deep convection increases LW and decreases SW radiation in the lower troposphere, with opposite effects in the mid

to upper troposphere. The compensating effects in LW and SW radiation are largely linked to variations in cloud fraction and water content (vapor, liquid and ice). These radiative balances in reanalyses are in agreement with idealized calculations using a column radiative transfer model. The overall relationships between OLR and diabatic heating are robust among the different reanalyses, although there are differences in radiative tendencies in the tropics due to large differences of cloud water and ice content among the reanalyses. These calculations provide a simple statistical method to quantify variations in diabatic heating linked to transient deep convection in the climate system.

Keywords Diabatic heating · Outgoing longwave radiation · Reanalyses · Cloud · Longwave · Shortwave

1 Introduction

Diabatic heating is a key driver of the atmospheric circulation and the global climate system. Diabatic heating originates from latent heating and radiative processes, and these separate components are linked with many aspects of the physical climate system. For example, large-scale moisture convergence and condensation, associated with latent heat release, are responsible for developing convective systems. Organized deep convection in the tropics is linked to variations in diabatic heating, which in turn drives circulations on large- and small-scales, including climatological monsoon structures, Hoskins and Rodwell (1995); El Niño Southern Oscillation (ENSO), Nigam et al. (2000); Madden–Julian Oscillation (MJO), Li et al. (2009) and mesoscale convective complexes, Houze (1989). Convection has strong and complex interactions with radiative heating due to diversity of cloud formations and convective

Electronic supplementary material The online version of this article (doi:10.1007/s00382-016-3501-0) contains supplementary material, which is available to authorized users.

✉ Kai Zhang
kzkaizhang@utexas.edu

¹ Jackson School of Geosciences, The University of Texas at Austin, Austin, TX, USA

² National Center for Atmospheric Research, Boulder, CO, USA

³ Dept. of Atmospheric & Oceanic Sciences, University of California, Los Angeles, CA, USA

behavior. A large amount of research has focused on quantifying diabatic heating associated with deep convection (e.g., Ling and Zhang 2013 and references therein) and developing corresponding parameterizations for large-scale numerical models (Bretherton 2007). A further use of diabatic heating rates is to drive vertical circulations in diabatic Lagrangian trajectory models; such calculations have been shown to be much less dispersive than corresponding kinematic calculations (based on diagnosed vertical winds) (e.g., Ploeger et al. 2010). Many studies have utilized diabatic heating rates to drive Lagrangian trajectory models to study the circulation and transport of different tracers, finding reasonable agreement with observations (Schoberl et al. 2012, 2013; Wang et al. 2014, 2015; Zhang et al. 2016). Such work has prompted detailed studies of diabatic heating rates from reanalysis data sets (e.g., Fueglistaler et al. 2009; Wright and Fueglistaler 2013). However, such analyses are typically focused on time average statistics, and there has been less emphasis on quantifying and comparing transient variability.

Deep convection in the atmosphere is complex and difficult to quantify in full detail. One common approach is to evaluate the space–time behavior of deep convection based on satellite measurements of Outgoing Longwave Radiation (OLR) (Ohring and Gruber 1983). Since June 1974, the operational National Oceanographic and Atmospheric Administration (NOAA) polar-orbiting satellites have provided OLR estimates from the window channel measurements of the Advanced Very High Resolution Radiometer (AVHRR) (Gruber and Krueger 1984; Gruber and Winston 1978; Liebmann and Smith 1996). In the tropics and mid-latitudes, variability of OLR is primarily linked to high-altitude clouds and deep convection and exhibits correspondingly complex behavior. Gridded OLR datasets, because of their continuous spatial and temporal coverage, have often been used to infer changes in the amount and height of clouds, intensity of precipitation and associated latent heating (e.g., Hu and Fu 2007; Park et al. 2007; Randel et al. 2015; Xie and Arkin 1998).

Convection in the atmosphere is linked to latent and turbulent heat fluxes linked with vertical diffusion, along with radiative processes [absorption of shortwave (SW) solar radiation and absorption/emission of longwave (LW) thermal radiation]. However, the links are complicated due to a high degree of transience and the broad spectrum of cloud and convective behavior. Diabatic heating rates including radiative and physical components, are difficult to measure directly. Modern meteorological reanalyses are widely used to derive the diabatic heat budgets. Comparisons of the heat

budgets among reanalyses have typically focused on the time average behavior, revealing some important differences, especially in the upper troposphere—lower stratosphere (UTLS) (Wright and Fueglistaler 2013). Fueglistaler et al. (2009) have compared the ERA-Interim diabatic heat budget with that of the older ERA-40 and found an overall better performance of ERA-Interim. Ling and Zhang (2013) have examined the diabatic heat budgets of three recent global reanalyses focused on levels in the troposphere, and found general agreements compared with results derived from available sounding observations based on wind and temperature fields, especially over the extratropics, where large-scale condensation dominates the rainfall processes.

In this paper we focus on quantifying transient variability of diabatic heating in reanalysis data products associated with observed fluctuations in convection, as identified in daily gridded OLR data. We use the OLR as a proxy of deep convection and cirrus/anvil clouds (in the tropics and middle latitudes), and quantify its correlations with daily variability in the separate diabatic heating rates, which are output as part of the meteorological reanalyses. We focus on the detailed results from ERA-Interim, but also include comparisons with JRA-55 and MERRA2. We separate the diabatic heating into components linked to ‘physics’ (mainly latent heating) and radiative (LW and SW) heating rates. In addition to global correlations, we use composites with respect to OLR to evaluate transient diabatic heating linked to moderate to extreme deep convection, with focus on the tropics and midlatitude storm tracks. We furthermore explore the variability in radiative fluxes using comparisons with an idealized column radiative transfer model, in order to explain the physical mechanisms behind the behavior derived from reanalysis data.

2 Data and methodology

Our analyses focus on diabatic heating fields derived from reanalyses. The total diabatic heating can be separated into physical and radiative components:

$$Q_{\text{total}} = Q_{\text{physics}} + Q_{\text{radiation}}$$

The radiation term can in turn be separated into two components, as longwave (LW) and shortwave (SW) radiative heating:

$$Q_{\text{radiation}} = Q_{\text{LW}} + Q_{\text{SW}},$$

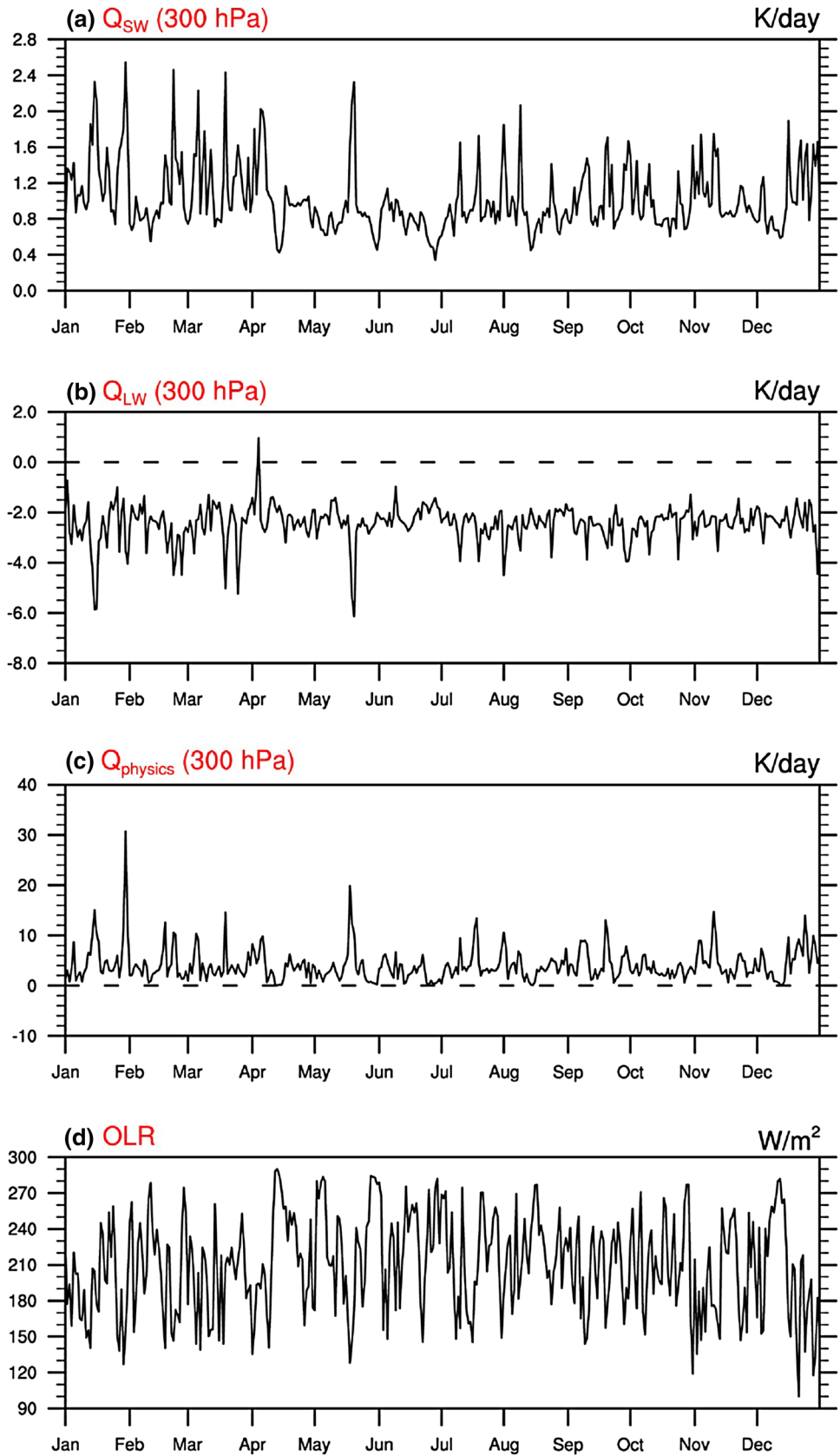
therefore

$$Q_{\text{total}} = Q_{\text{physics}} + Q_{\text{LW}} + Q_{\text{SW}}.$$

The radiation term can also be broken into clear-sky and cloud radiative heating:

$$Q_{\text{radiation}} = Q_{\text{clear}} + Q_{\text{cloud}} = (Q_{\text{LW_clear}} + Q_{\text{SW_clear}}) + (Q_{\text{LW_cloud}} + Q_{\text{SW_cloud}}).$$

Fig. 1 Example time series at grid point (0°, 150°E) during year 2003 for **a** Q_{SW} ; **b** Q_{LW} ; **c** $Q_{physics}$ at 300 hPa and **d** OLR. Note the different vertical scales in **a–c**



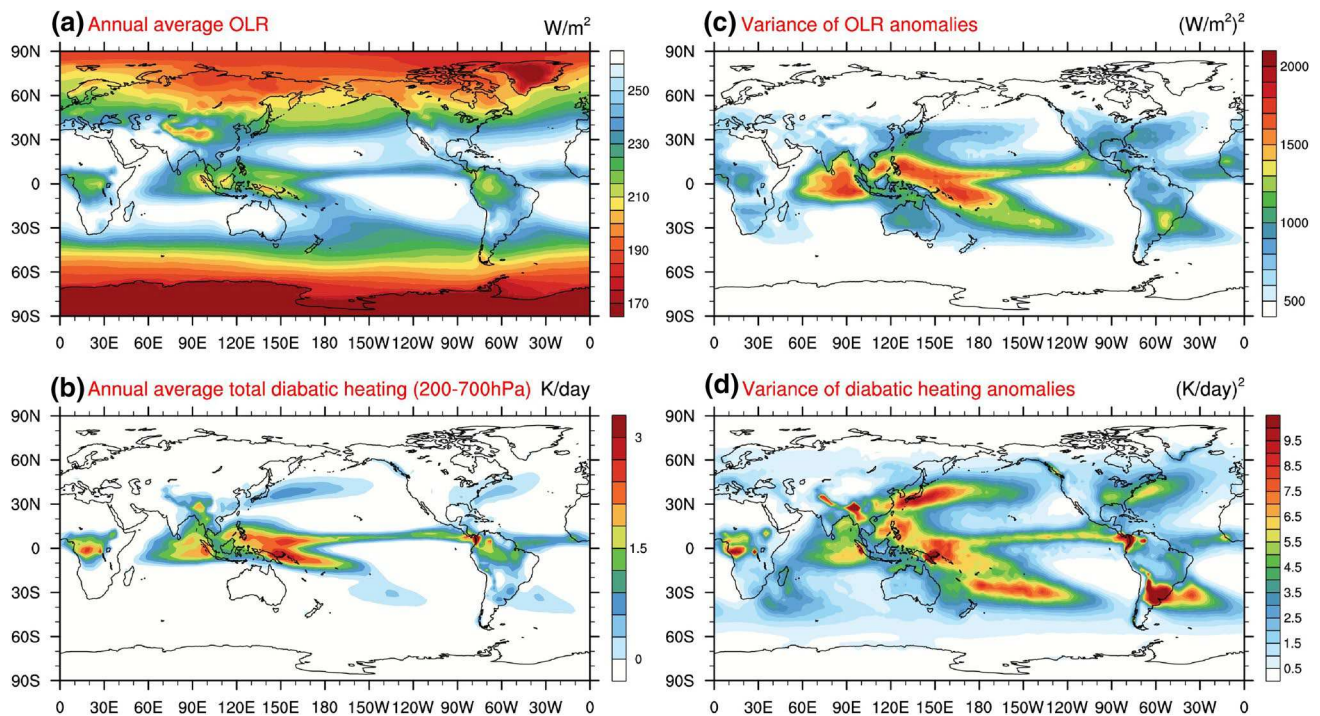


Fig. 2 Left panels are annual averaged **a** OLR and **b** vertically averaged Q_{total} between 200 and 700 hPa in ERA-Interim. *Right panels c, d* show variance maps for their respective anomalies. Note that the *color bar* is reversed in **a**

The separate clear and cloud radiative terms are provided in the reanalyses, and these can be used to quantify cloud radiative effects.

In the following, we will compare the global behavior of diabatic heating with daily gridded OLR data. We quantify the variabilities of the separate diabatic heating components (Q_{total} , Q_{physics} , $Q_{\text{radiation}}$, Q_{LW} and Q_{SW}) and their correlation with OLR, and examine detailed vertical structures based on composited values. The clear-sky and cloud radiative heating are also used to identify the effects of cloud on radiative heating. We focus on results based on ERA-Interim diabatic heating rates, and include the results from JRA-55 and MERRA2 reanalyses in the supplementary materials.

ERA-Interim is a reanalysis spanning from 1979 to present (Dee et al. 2011). Output of the reanalyses includes total diabatic heating, plus separate components due to longwave (LW) and shortwave (SW) radiative heating. Heating rates due to physical processes (‘physics’) are not provided directly but can be derived as a difference between the total heating and radiative components. The physics heating term in the ERA-Interim is due to latent heating (primarily moist physics) and heating associated with turbulent mixing (Fueglistaler et al. 2009): $Q_{\text{physics}} = Q_{\text{latent}} + Q_{\text{turbulent}}$. Since these two separate components are not provided in ERA-Interim, we cannot quantify their individual behaviors. An example of time series

of OLR and several components of heating at one specific grid point (0° , 150°E) during 1 year (2003) is shown in Fig. 1. OLR shows large day-to-day variations, linked to transient deep convection and high clouds (low OLR) at this location. Note that extreme convection in the deep tropics is associated with OLR $< 180 \text{ W/m}^2$. There are large corresponding daily variations in Q_{physics} , Q_{LW} and Q_{SW} in Fig. 1, which are correlated with OLR and with each other (note that Q_{LW} and Q_{SW} are often anti-correlated, which is typical, as shown below). Our analyses are aimed at quantifying the relationships among these variables over the globe, including their detailed vertical structure.

MERRA2 reanalysis has been produced by NASA’s Global Modeling and Assimilation Office (GMAO) of NASA based on the Goddard Earth Observing System, version 5 (GEOS-5) (Rienecker et al. 2011), covering the satellite era (1980–present). MERRA-2 is the newest reanalysis product updated from MERRA reanalysis (Bosilovich et al. 2015). The development of MERRA2 includes assimilating additional observations and improving the data assimilation model and observing system (Molod et al. 2015). MERRA2’s diabatic heating includes components of heating due to LW radiation, SW radiation, moist physics, turbulent mixing, gravity wave drag, and friction (which we combine into a total physics term).

The Japanese 55-year reanalysis (JRA-55) is the second Japanese global atmospheric reanalysis conducted by the

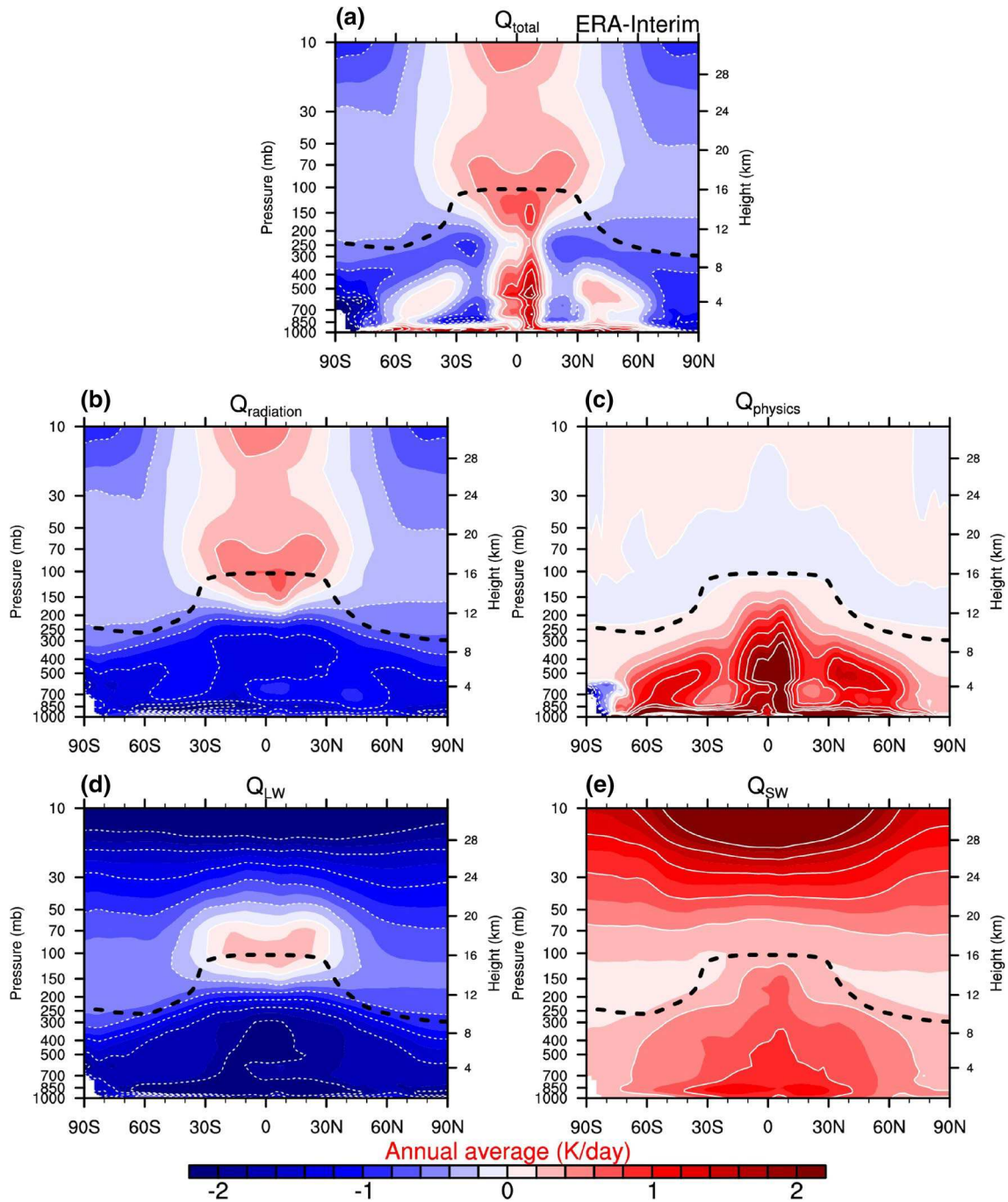


Fig. 3 Zonal mean diabatic heating averaged over the period of 1979–2013 for **a** Q_{total} ; **b** $Q_{radiation}$; **c** $Q_{physics}$; **d** Q_{LW} ; **e** Q_{SW} in ERA-Interim. The black dashed lines denote the tropopause

Japan Meteorological Agency (JMA), covering the period of 1979–present (Kobayashi et al. 2015). The JRA-55 provides heating rates due to LW radiation, SW radiation, convection, large-scale condensation and vertical diffusion (which we combine into a total physics term).

NOAA interpolated OLR daily gridded analyses are obtained from NOAA-Cooperative Institute for Research in

Environmental Sciences Climate Diagnosis Center (<http://www.cdc.noaa.gov/>). The OLR flux is estimated from IR window channel brightness temperatures based on a non-linear regression in comparisons to broadband earth radiation budget observations (Ohring et al. 1984) for day and night separately. The total OLR flux for a month is obtained by averaging all nighttime and daytime estimates within the

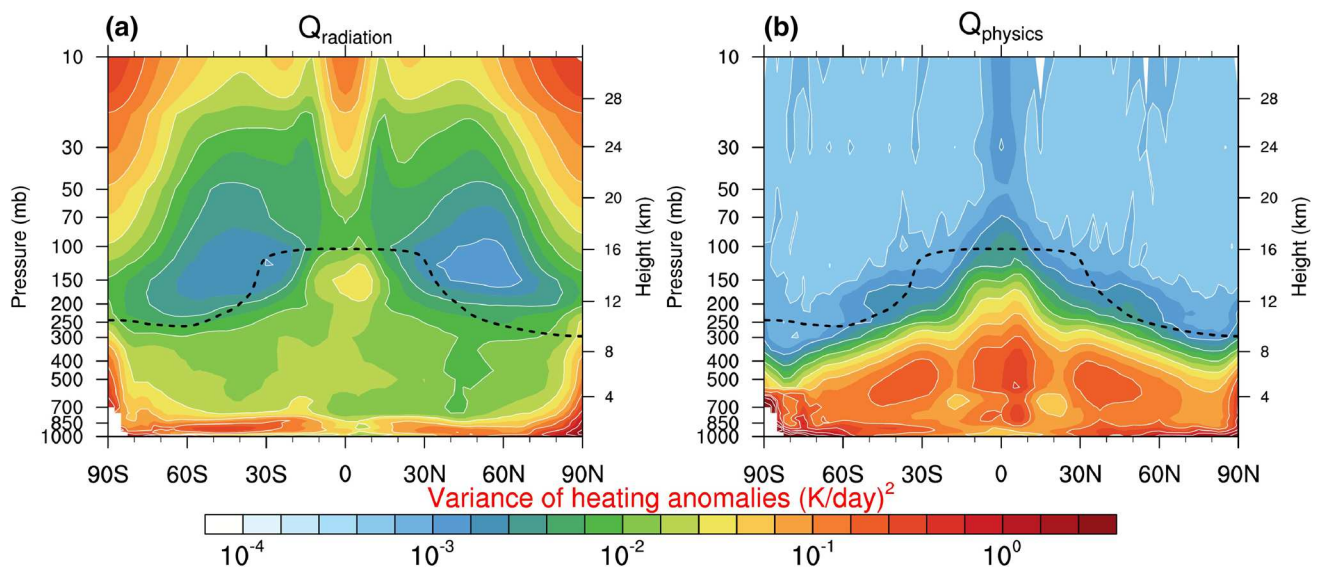
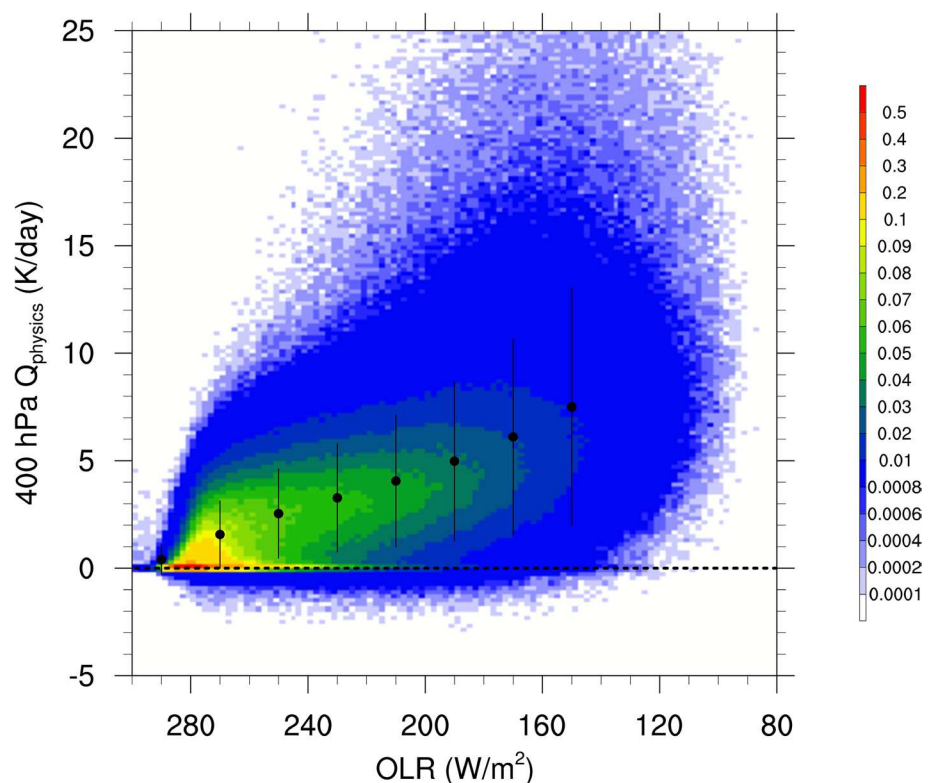


Fig. 4 Total variance of anomalies of **a** $Q_{\text{radiation}}$; **b** Q_{physics} as a function of latitude and pressure in ERA-Interim. Note the logarithmic color scale. The black dashed lines denote the tropopause

Fig. 5 Scatter plot of daily Q_{physics} at 400 hPa and OLR in the tropical western Pacific (within the box shown below in Fig. 10). The black dots represent the composite mean and the vertical black lines represent the standard deviation intervals of Q_{physics} at different OLR levels



period. We have regridded the daily reanalysis heating rates onto the same horizontal grid ($2.5^\circ \times 2.5^\circ$) as OLR data. The correlation calculations are based on daily anomalies in the period of 1979–2013, which are derived by subtracting 35-year averaged seasonal cycle from the original time series at each grid point (for both OLR and the individual diabatic heating rates).

We note that OLR is also a diagnostic provided by the different reanalyses. We choose to use the observed (NOAA) OLR product in this work, in order to link our results to other studies based on observed OLR, and to have a common reference (transfer standard) among reanalyses. Very similar overall results are found using reanalysis OLR.

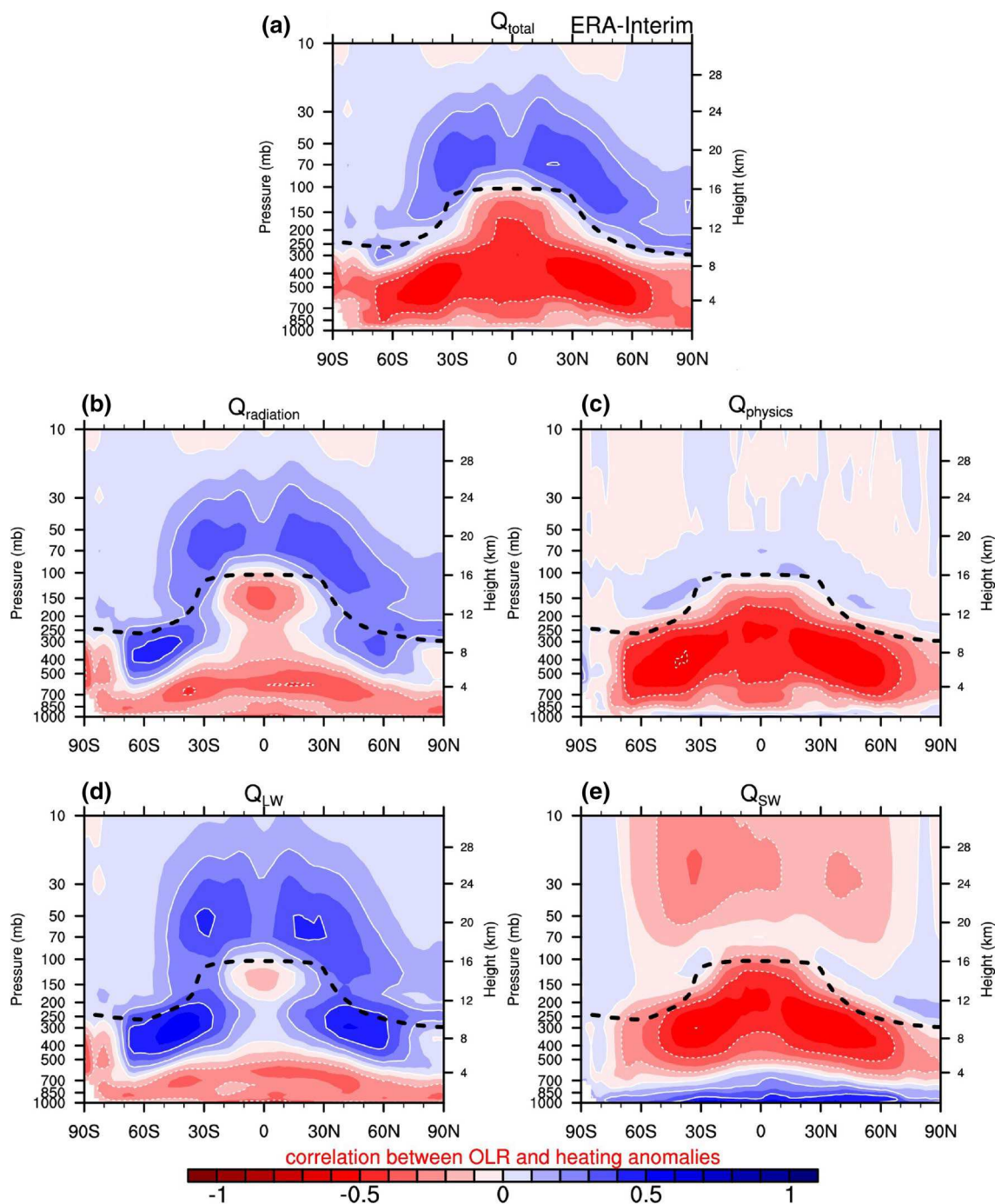


Fig. 6 Zonal average of correlations between OLR and anomalies of **a** Q_{total} ; **b** $Q_{radiation}$; **c** $Q_{physics}$; **d** Q_{LW} and **e** Q_{SW} in ERA-Interim. The correlations are calculated at each latitude/longitude grid point and

then zonally averaged. The sense of the color scale is that enhanced convection is linked to diabatic heating (red) or cooling (blue). The black dashed lines denote the tropopause

3 Results

3.1 Annual average and variability of OLR and diabatic heating

The annual averages of OLR and vertically averaged Q_{total} between 200 and 700 hPa during 1979–2013 are shown in

Fig. 2a, b. Persistent deep convection in the tropics is associated with time average low OLR and positive Q_{total} . The global patterns show that while low OLR is an indicator of strong convection in tropics, it does not necessarily imply deep convection over high latitudes (Fig. 1a), where the low values are largely due to the cold surface and atmospheric temperatures. In contrast, the time average Q_{total}

distribution captures the deep convection over tropics, and also convective patterns over the storm track regions in the mid-latitudes. Maps of the variances of (deseasonalized) OLR and Q_{total} (Fig. 2c, d) show consistent spatial patterns, with largest variability over tropical convective regions and storm tracks in the mid-latitudes, and smallest variability over the polar regions. Note that Q_{total} shows relatively stronger variability than OLR over the storm track regions.

The annual and zonal averages of diabatic heating profiles for each component based on ERA-Interim are shown in Fig. 3 (profiles based on JRA-55 and MERRA2 are shown in Fig. S1 in the supplementary materials). In the troposphere, the time average balance is primarily between heating from Q_{physics} and net radiative cooling; the total diabatic heating shows a net heating in tropics and mid-latitudes and cooling in subtropics (Fig. 3a), which is presumably balanced by circulation effects. Maximum tropospheric heating is associated with strong latent heat release by convection in the tropics and storm tracks (over $\sim 30^{\circ}$ – 60° N/S, Fig. 3c). The net radiative cooling in the troposphere is a balance of LW cooling and (weaker) SW warming. In the stratosphere,

the total diabatic heat budget is dominated by the radiative component (Fig. 3b), with heating in the tropics and cooling in the extratropics (balanced by the mean overturning Brewer–Dobson circulation, BDC). The LW radiative component in Fig. 3d shows cooling throughout the troposphere and stratosphere, except for heating in the tropical tropopause layer (TTL), which is linked to the low temperatures (below radiative equilibrium) maintained by the mean upward BDC. The SW radiative tendencies show a global heating with greatest values in the stratosphere (due to ozone absorption) and lower-middle troposphere (due to water vapor and cloud absorption), weakening from tropics to high latitudes, corresponding to the distribution of incoming solar radiation and water vapor content. In the troposphere and the extratropical stratosphere, LW cooling exceeds SW heating, while in the tropical stratosphere SW heating is larger than LW cooling. In the TTL, both LW and SW radiative components contribute heating, consistent with Gettelman et al. (2004). The combination of LW and SW components gives the time average radiative heating pattern in Fig. 3b.

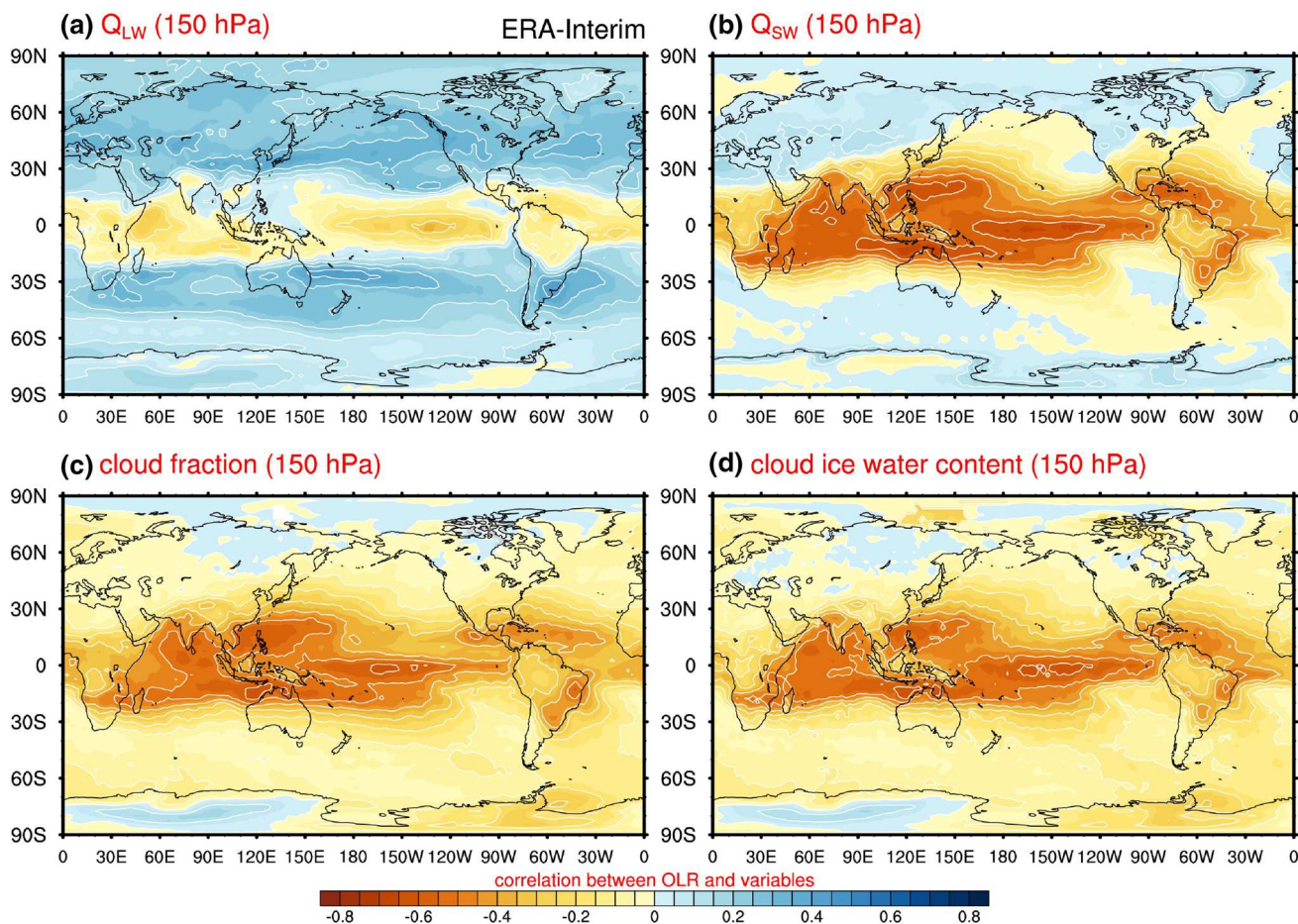


Fig. 7 Maps showing local correlations between OLR anomalies and **a** Q_{LW} , **b** Q_{SW} , **c** cloud fraction, and **d** cloud ice water content at 150 hPa

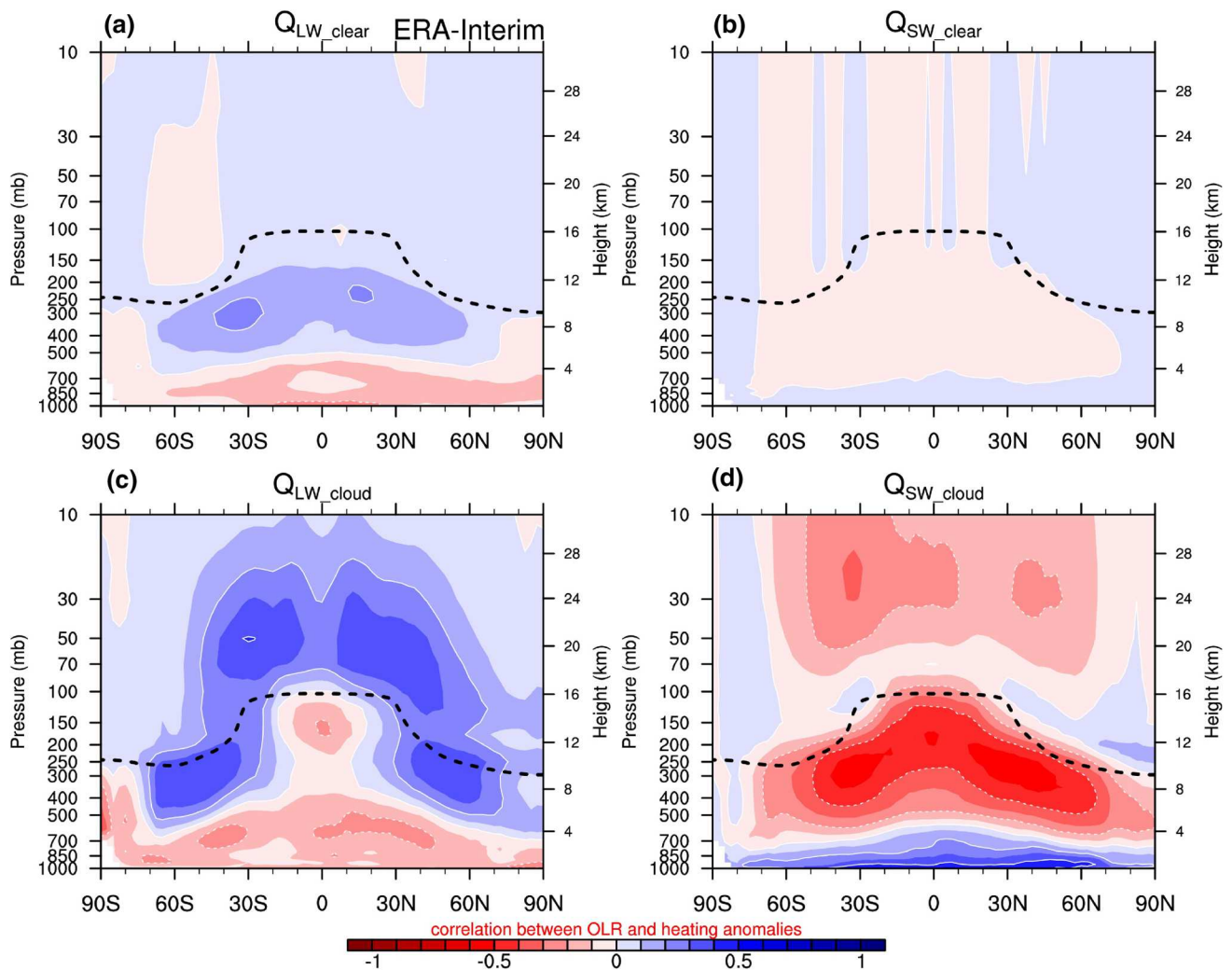


Fig. 8 Zonal average of correlations between OLR and anomalies of **a** Q_{LW_clear} ; **b** Q_{SW_clear} ; **c** Q_{LW_cloud} and **d** Q_{SW_cloud} in ERA-Interim. The sense of the color scale is that enhanced convection is linked

to diabatic heating (red) or cooling (blue). The black dashed lines denote the tropopause

Maps of the temporal variances of diabatic heating for radiative ($Q_{radiation}$) and physical components ($Q_{physics}$) are shown in Fig. 4, showing zonal averages of variances calculated at each longitude. In the troposphere, the variability of the total diabatic heating is dominated by the physical component in Fig. 4b, with maxima associated with tropical convection and storm tracks (as seen in Fig. 3c). There is also large variance in $Q_{radiation}$ near the surface. In the stratosphere the variability of the total diabatic heating is dominated by the radiative component (Fig. 4a), primarily from the LW radiative heating (tied to temperature variations). There are relative stratospheric variance maxima over the equator for both $Q_{radiation}$ and $Q_{physics}$, linked to temperature and wind shear (turbulence) anomalies associated with the stratospheric quasi-biennial oscillation (QBO).

3.2 Correlations between OLR and diabatic heating

Our analyses use OLR as a proxy for convective activity, and we anticipate close statistical relationships with diabatic heating (although the overall variations are complex in all fields). To illustrate this variability, Fig. 5 shows the statistical distribution of $Q_{physics}$ at 400 hPa vs. OLR, for sampling in the tropical western Pacific (within the box shown below in Fig. 10). The main part of the distribution shows a clear relationship between low OLR and enhanced $Q_{physics}$, and this behavior is quantified by the binned values of $Q_{physics}$ indicated in Fig. 5. Such average relationships between Q and OLR are the focus of our analyses, although there is also a rich spectrum of variability not simply related to OLR. In addition, Fig. 5 shows a broad

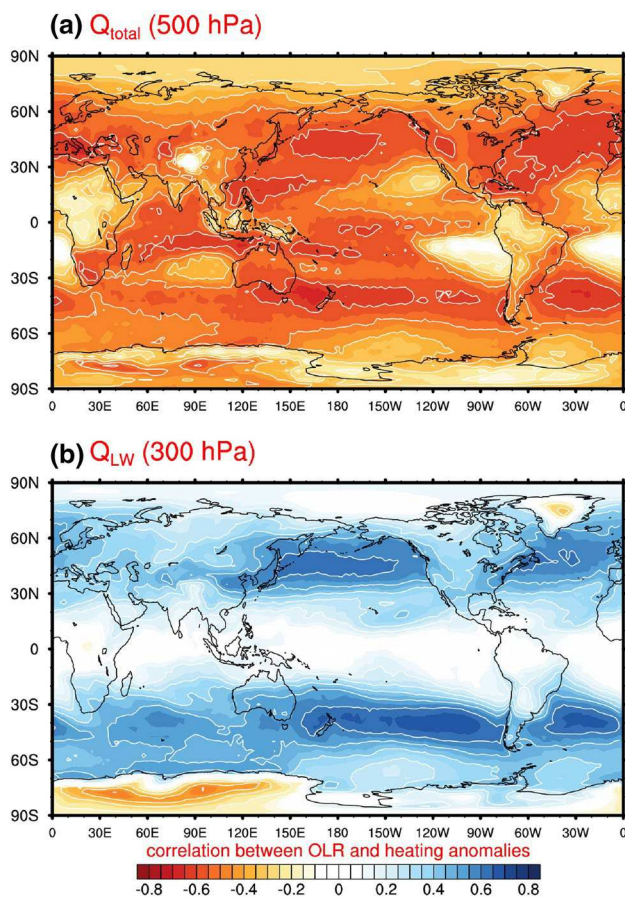


Fig. 9 Maps showing correlations between OLR anomalies and a Q_{total} at 500 hPa and b Q_{LW} at 300 hPa

distribution in both Q_{physics} and OLR, with (infrequent) occurrence of high Q_{physics} (>15 K/day) and very low OLR (<160 W/m²).

The correlation patterns between OLR and diabatic heating anomalies of each component are shown in Fig. 6 (zonal means of correlations calculated at each longitude). Red shading indicates negative correlation, such that intensified convection (lower OLR) is associated with enhanced heating; likewise, blue shading indicates cooling with enhanced convection.

The overall patterns of correlations for Q_{total} (Fig. 6a) show that enhanced convection is linked to diabatic heating throughout the troposphere and cooling in the lower stratosphere. The tropospheric warming is primarily tied to correlation with physics terms (Fig. 6c; mainly latent heating). The net radiative response in the troposphere is a balance of LW and SW effects (shown separately in Fig. 6d, e). Enhanced convection is tied to relative SW cooling (reduced warming) near the surface, together with warming throughout the rest of the troposphere, due to cloud and water effects on SW radiation (e.g., Fung and Ramaswamy 1999). Conversely, transient convection

produces relative LW warming (weaker cooling) at low levels (below ~ 5 km) and enhanced cooling in the upper troposphere, especially over middle latitudes. There is a weaker correlation with Q_{LW} in the tropical upper troposphere compared to midlatitudes. In the troposphere, the LW variations dominate over SW, so that correlations for the net radiative heating (Fig. 6b) are similar to LW alone. As shown below, much of the coherent variations in tropospheric SW and LW fluxes linked to convection can be explained by associated variations in cloud fraction and cloud water and ice content. Enhanced convection tends to warm the TTL (~ 100 – 150 hPa), primarily from Q_{SW} (and a weak contribution from Q_{LW}), although this is a detail that is specific to ERA-Interim (as discussed below). The local behaviors of these correlations (at 150 hPa) are shown in Fig. 7, together with corresponding correlations with cloud fraction and cloud ice water content. Figure 7 shows that in the TTL the response of Q_{SW} to deep convection is closely linked with the behaviors of cloud fraction and ice content.

The net response of the stratosphere to increased convection is radiative cooling (Fig. 6a, b). Deep convection increases SW heating in the stratosphere (Fig. 6e), due to increases in reflected SW from high clouds, and absorption by stratospheric ozone. However, enhanced convection causes stronger stratosphere LW cooling (Fig. 6d), due to weaker LW tropospheric emission in situations of high cloud (e.g., Fueglistaler and Fu 2006; Hartmann et al. 2001). The LW component dominates over the SW, so that the total radiative effect is cooling (Fig. 6b). The strongest LW stratospheric correlation patterns occur over lower latitudes ($\sim 30^\circ\text{N}$ – S), with a slight minimum over the equator.

The correlation patterns between OLR and the separate clear-sky and cloud radiative heating anomalies of Q_{LW} and Q_{SW} are shown in Fig. 8. The overall relationships between OLR and radiative heating in Fig. 6d, e are mostly due to cloud radiative effects (Fig. 8c, d), with corresponding large variability in OLR. The effects of cloud properties on radiative heating will be further studied in Sect. 3.4. Clear-sky Q_{LW} shows weak OLR correlations (Fig. 8a), indicating cooling in the upper troposphere and heating in the lower troposphere linked with lower OLR. This behavior mainly occurs for relatively high values of OLR over clear regions (not tied to deep convection), and is primarily linked to variations in atmospheric water vapor in these regions. There are not significant correlations between OLR and clear-sky Q_{SW} .

Almost all of the correlation patterns seen in Fig. 6, based on ERA-Interim data, are similar to results based on JRA-55 and MERRA2 reanalyses (Figure S2), except for some detailed differences in the radiative responses in the tropics. These are described below.

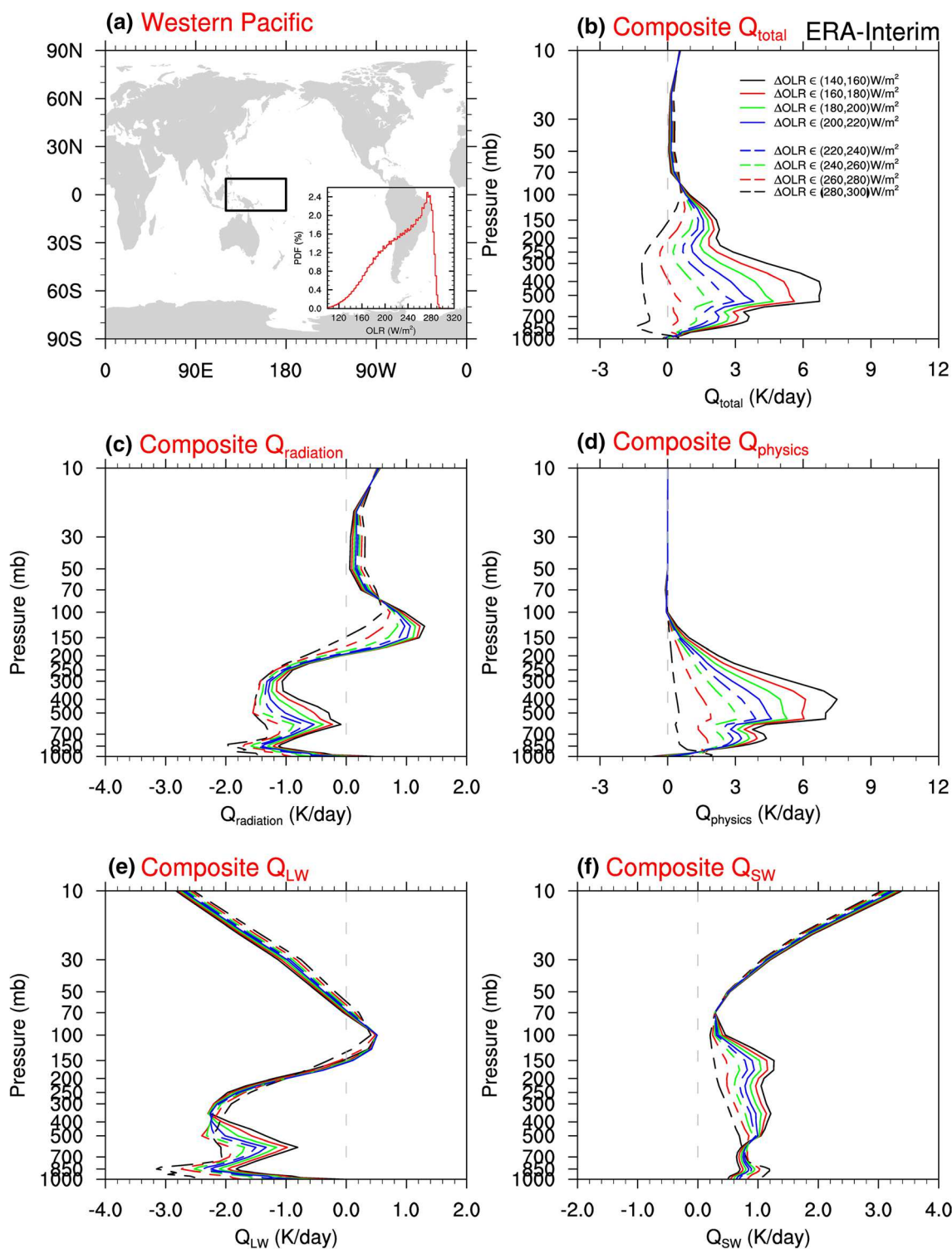


Fig. 10 Diabatic heating profiles composited according to co-located OLR values for **b** Q_{total} ; **c** $Q_{radiation}$; **d** $Q_{physics}$; **e** Q_{LW} ; and **f** Q_{SW} . **a** The selected region over western Pacific (10°S–10°N, 120°–180°E) for composite analysis. Binned OLR values vary from the category of

280–300 (dashed black line hereafter) to 140–160 (black line hereafter) W/m². Note that the scales of x-axis in **b** and **d** are different from those in **c**, **e**, **f**. Red curve in **a** is the probability density distribution of OLR in this region

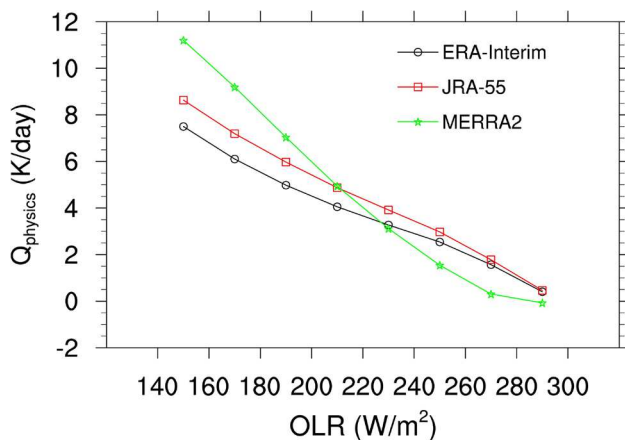


Fig. 11 Variations of tropical diabatic heating from Q_{physics} from the three reanalyses, binned as a function of OLR. These results are from the Western Pacific, using values at 400 hPa (near the altitude maximum in Q_{physics})

The spatial patterns of the correlation between OLR and Q_{total} anomalies in the troposphere (500 hPa) is shown in Fig. 9a. The strongest negative correlations for Q_{total} occur over the tropics and storm track regions in the mid-latitudes (especially over the oceans), related to the latent heating (moist physics) from convection. Minimum correlations occur only over regions that are devoid of deep convection, to the west of the continents in the subtropics. The correlations between OLR and Q_{LW} in the upper troposphere (300 hPa) are highlighted in Fig. 9b, showing strongest response over the mid-latitude oceanic regions. This behavior is tied to convection-related water content and cloud variations, which have a strong LW cooling effect.

3.3 Composite diabatic heating based on OLR values

To quantify the response of diabatic heating to OLR changes over different regions in more detail, we show diabatic heating profiles from ERA-Interim composited for different values of co-located OLR (corresponding to varying altitude of cloud top and intensity of convection). We simply bin the diabatic heating in localized regions for various OLR values in 20 W/m^2 bins, spanning from below 160 W/m^2 (extreme deep convection) to above 280 W/m^2 (no convection), e.g. see Fig. 5. These composites quantify the magnitude and vertical profile of the diabatic heating variations tied to convection. We focus on two examples, over the western Pacific (tropical convective region, Fig. 10) and northwestern Pacific (mid-latitude storm track region, Fig. 12).

Over the western Pacific, enhanced convection is linked to latent heat response with a broad vertical scale spanning ~ 700 – 200 hPa, with a maximum near 400 hPa (Fig. 10d). This behavior is similar to previous estimates of diabatic

heating in deep convection, e.g. Ling and Zhang (2013), and references therein. The heating amplitude for strongest convection ($\text{OLR} < 180 \text{ W/m}^2$) is ~ 6 K/day in the middle troposphere (Fig. 10d), although individual peaks can be substantially stronger (Figs. 1, 5). Variations in $Q_{\text{radiation}}$ (Fig. 10c) show that enhanced convection is tied to stronger warming near 150 hPa, mainly as a result of increased Q_{SW} , and decreased cooling near 700 hPa, due to Q_{LW} . The variations in Q_{LW} and Q_{SW} with respect to OLR are a convolution of clear sky and cloud effects; clear-sky Q_{LW} is dominated by variations in water vapor and cloudy Q_{LW} by liquid water and ice (as shown below).

Comparisons of these results among the reanalyses show similar patterns and magnitudes for Q_{physics} in the tropics (c.f. Figs. 10 and S3), but with some interesting systematic differences in maximum amplitude. Figure 11 compares the composited values of Q_{physics} near the tropical maximum (400 hPa) versus OLR for the three reanalyses, showing systematically stronger heating for the most intense convection ($\text{OLR} < 200 \text{ W/m}^2$) for MERRA2, followed by JRA55 and ERA-Interim. The differences are relatively large for the most intense convection. Conversely, MERRA2 shows smaller heating rates for higher OLR values. These differences might be expected to influence the transient thermodynamic balances in the respective reanalyses.

Composited variations in diabatic heating rates over the northwestern Pacific storm track are shown in Fig. 12. Heating from Q_{physics} (Fig. 12d) peaks in the middle troposphere, centered slightly lower than the corresponding maximum in the tropics (Fig. 10d), with somewhat smaller maximum values. Very similar behavior is seen with MERRA and JRA-55 statistics (Fig. S4). Changes in Q_{LW} and Q_{SW} show dipole patterns in the vertical between the lower and upper troposphere, with compensating effects between SW and LW components; the net result is stronger cooling in the upper troposphere and weaker cooling in the lower troposphere for enhanced convection (Fig. 12c). The clear influence of deep convection on stratospheric LW cooling is also evident in Fig. 12e.

3.4 Convective effects on water content, clouds and radiation response

As shown in Fig. 8c, d, the coherent variations of Q_{LW} and Q_{SW} response to deep convection seen in the above statistics can be understood to a large degree as a response to corresponding changes in cloud fraction and water and ice content. We evaluate this behavior by quantifying the related cloud variations in the reanalyses tied to convection, and then studying the corresponding radiative effects based on a column radiation model.

Variations in convection are strongly correlated with the vertical distributions of cloud fraction, liquid and ice water

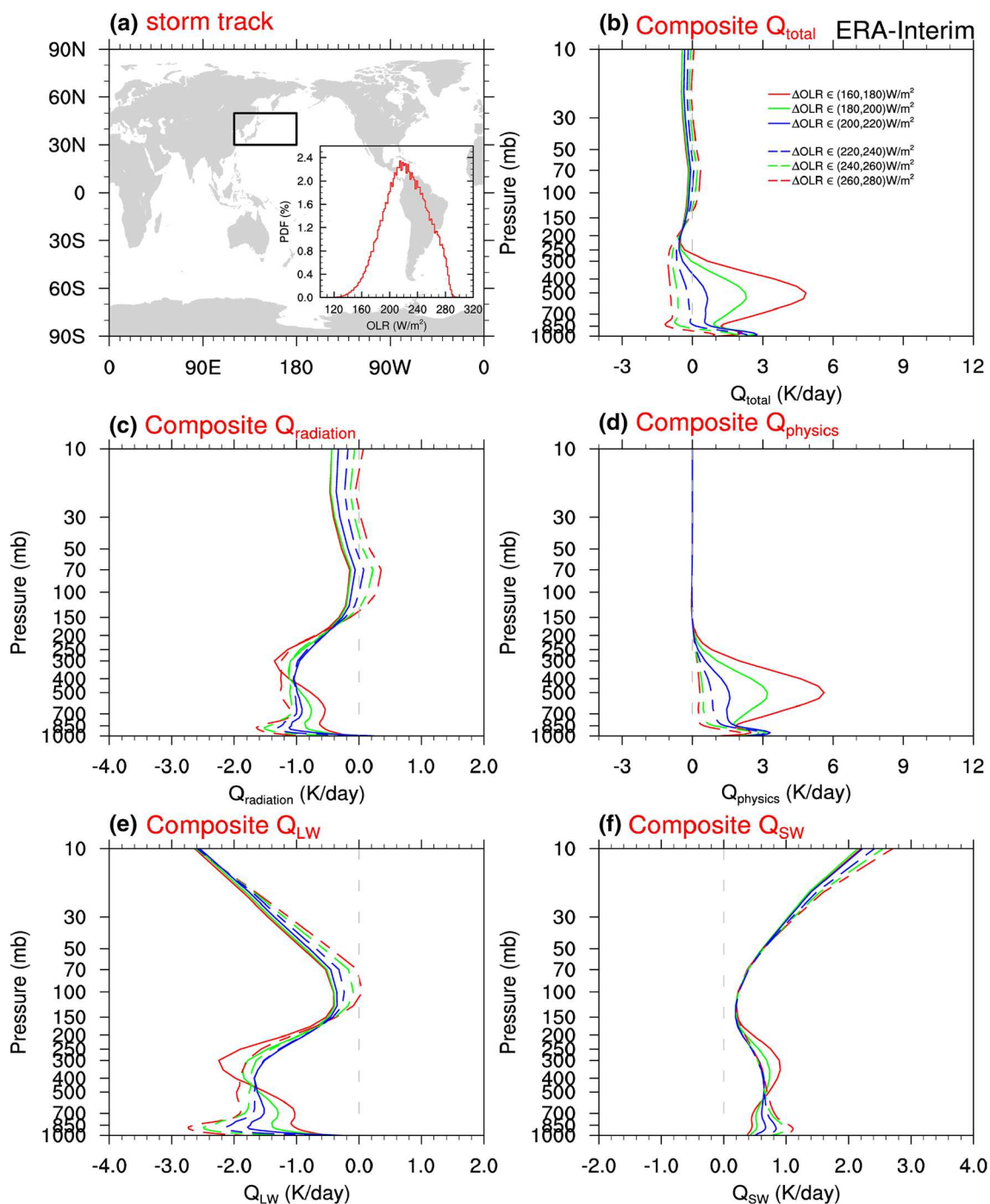


Fig. 12 Diabatic heating vertical profiles composited according to co-located OLR over the northwestern Pacific (30°–50°N, 120°–180°E). Details are the same as in Fig. 10

content over tropics and middle latitudes. This behavior is expected, simply from the cloud formation and condensation processes in convective systems. The calculated correlations between OLR and ERA-Interim cloud fields are shown in Fig. 13, for statistics at 500 hPa (cloud fraction and ice water content) and 700 hPa (cloud liquid water content). There are strong correlations between OLR and

cloud behavior (as expected), and these figures emphasize variability in the mid-latitude oceanic storm track regions. Corresponding variations in cloud fraction and ice water content at 150 hPa were shown in Fig. 8c, d, emphasizing similar strong relationships with convection in the tropics.

Figure 14 shows composited cloud vertical profiles as a function of OLR for the western Pacific and storm

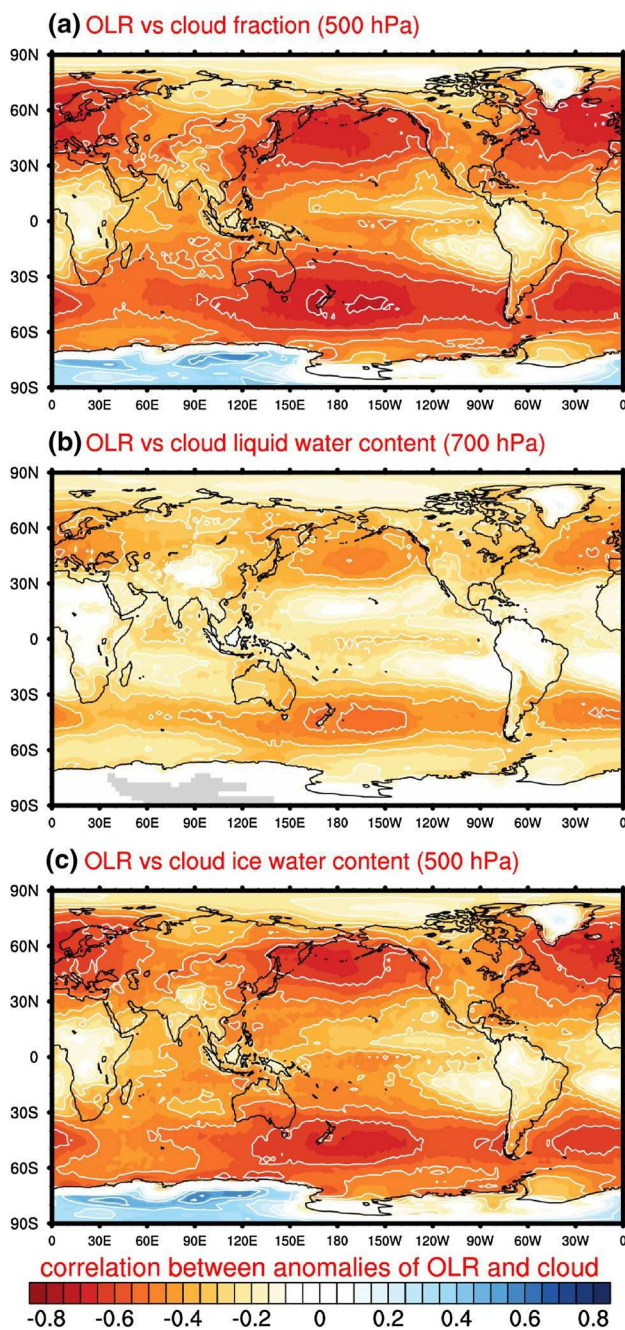


Fig. 13 Correlations between OLR and cloud fraction at 500 hPa (*top panel*), cloud liquid water content at 700 hPa (*middle panel*), and cloud ice water content at 500 hPa (*bottom panel*) in ERA-Interim

track regions. Over the western Pacific, the response of cloud fraction maximizes near 150 hPa (Fig. 14a; see also Fig. 8c), corresponding to intense deep convection in this region. This pattern occurs higher than the response over the storm track region, which maximizes near 400 hPa (Fig. 14b). The cloud liquid water content profiles show double peaks at 500 and 850 hPa over the western Pacific. The magnitude of the response is stronger over the storm

track region. The composited cloud ice water content peaks at similar level (~ 400 hPa) over the two regions, but extends to higher altitudes over the western Pacific.

The radiative responses to these variations in cloud behavior are evaluated using an accurate column radiative transfer model (RRTM) (Iacono et al. 2000; Mlawer et al. 1997). RRTM was developed by Mlawer et al. (1997) and provided by the Atmospheric and Environmental Research Inc. It utilizes the correlated-k approach to calculate fluxes and heating rates efficiently and accurately. We use the respective vertical profiles of climatological mean temperature and water vapor as input to the RRTM, and test the responses to variations in cloud fraction, plus liquid and ice water content, as derived in Fig. 14. Both diurnal and annual cycles have been averaged in the calculation of SW heating rates. The effective radii of ice crystals and liquid droplets are set to 45 and 15 μm , respectively. We note that the vertical profiles of the SW heating rates in the RRTM are sensitive to the parameters of ice crystal and liquid droplet sizes.

Figure 15 shows variations in Q_{LW} and Q_{SW} output from the RRTM as a response to the cloud variations in the western Pacific and storm-track region shown in Fig. 14. The results can be compared with the reanalysis sensitivities shown in Figs. 10e, f and 12e, f. The results over the storm track region show out-of-phase variations in Q_{LW} the upper and lower troposphere, and compensating changes in Q_{SW} , very similar to the behavior derived from the reanalysis data in Fig. 12e, f. Variations in cloud fraction and liquid water content are the most important contributors to this behavior. The RRTM results over the western Pacific show similar vertical profiles and sensitivities to the ERA-Interim statistics in Fig. 10e, f, although the variations in Q_{SW} in the upper troposphere are much smaller in RRTM. Note that the LW heating rates in the tropical upper troposphere show less sensitivity to cloud variations than those in the storm track region (in both RRTM and ERA-Interim); this behavior gives rise to the tropical upper tropospheric minimum in Q_{LW} correlations seen in Fig. 6d. Overall there is reasonable quantitative agreement with the RRTM calculations, demonstrating that variations in cloud fraction and water and ice content are key factors influencing the tropospheric radiative heating balances tied to convection.

There are substantial differences in the tropical Q_{LW} and Q_{SW} responses to convection in the tropics among the reanalyses, which are reflected in the correlation and composite patterns. Vertical profiles of composited Q_{LW} and Q_{SW} for the western Pacific from JRA-55 and MERRA2 are shown in Fig. 16 (for comparison to the ERA-Interim results in Fig. 10e, f). JRA-55 is similar to ERA-Interim, while MERRA2 shows more complex vertical structure for Q_{LW} and larger sensitivity to

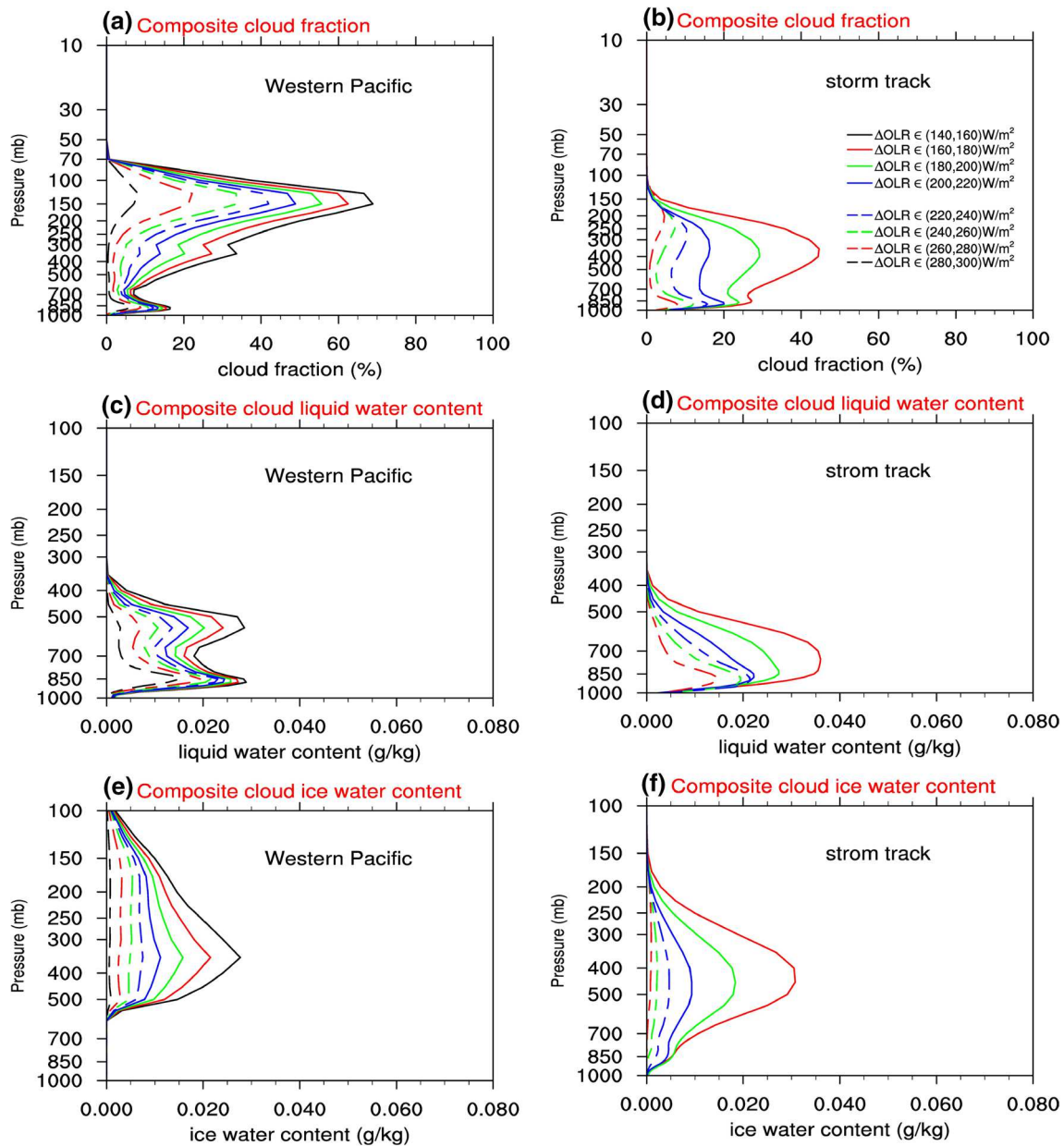


Fig. 14 Vertical profiles of cloud fraction (*top panel*), cloud liquid water content (*middle panel*) and cloud ice water content (*bottom panel*) composited according to co-located OLR, for statistics in the western Pacific (*left panel*) and storm track (*right panel*) regions

deep convection for Q_{SW} in the upper troposphere. These sensitivities probably reflect large differences in corresponding cloud water and ice content between the reanalyses, as shown in Fig. 17. The cloud liquid water content profiles for JRA-55 show a single peak at ~ 800 hPa, and three peaks at ~ 350 , 600 and 850 hPa in MERRA2; MERRA2 has much larger water content above 500 hPa than either JRA-55 or ERA-Interim. The cloud ice content is also very different, with approximately an order of magnitude difference between JRA-55 and MERRA2 (Fig. 17), with ERA-Interim values between the two (Fig. 14e). These large differences in cloud water and ice

content are probably the main cause of the very different tropical radiative heating rates among the reanalyses (Fig. 16). Similar comparisons in the storm track region do not show such large differences, but rather overall agreement in cloud statistics and radiative responses.

4 Conclusions and discussion

We have used the ERA-Interim reanalyses to investigate the variability of diabatic heating and its relationships with transient deep convection (using OLR as a proxy for

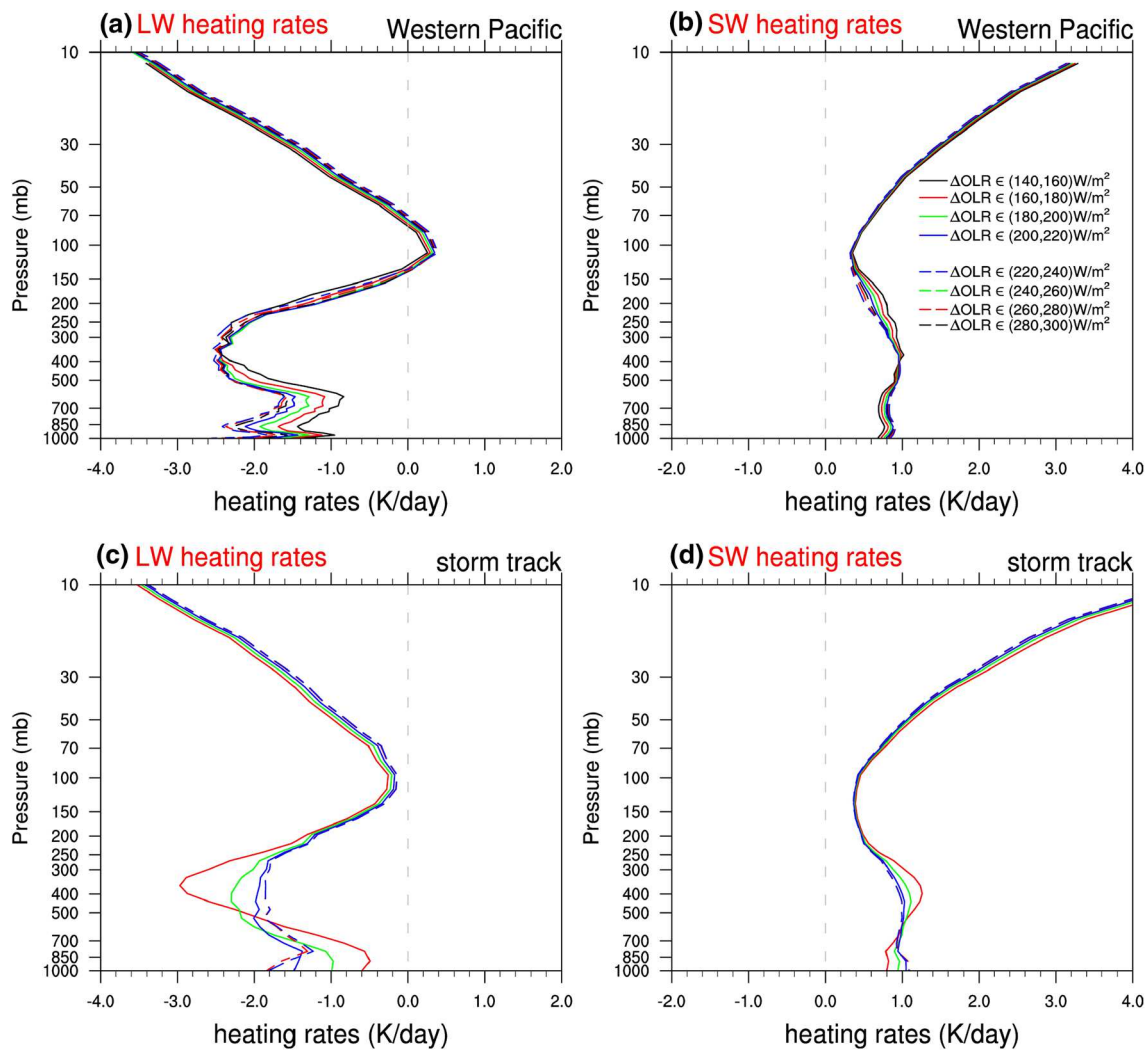


Fig. 15 Heating rate variations derived from the RRTM column radiation model, incorporating the observed cloud changes in Fig. 14. Results are shown for the western Pacific (*top panels*) and storm track regions (*bottom panels*), including LW (*left*) and SW (*right*) heating rates

observed convection). We propose this as a simple statistical method to investigate the coherent behavior in diabatic heating profiles associated with highly variable and complex changes in deep convection. Although most of the illustrated results are based on ERA-Interim reanalysis, we derive similar results based on JRA-55 and MERRA2 reanalysis. While there are differences in the time average diabatic heating rates among different reanalyses (e.g., Ling and Zhang 2013; Wright and Fueglistaler 2013), we find that the overall statistical links between observed OLR and diabatic heating rates are not strongly dependent on which reanalysis is used (aside from the radiative tendencies in the tropics).

In the troposphere, the dominant variability of diabatic heating is tied to latent heating, which is parameterized in large-scale models. Our analyses find strong correlations between latent heating and OLR over the tropics and storm

track regions, which is reasonable and consistent with previous analyses (e.g., Ling and Zhang 2013). Composited values show that the magnitude of tropical diabatic heating linked to the strongest convection is somewhat different among the reanalyses (Fig. 11). In the stratosphere diabatic heating is dominated by the radiative components, and we find enhanced LW radiative cooling tied to tropospheric convection. This relationship in the stratosphere is consistent with the study of Norton (2001), who showed anticorrelation between upper tropospheric cloud cover and lower stratospheric heating rates in ECMWF data, which was interpreted as a consequence of the reduced LW heating in the lower stratosphere in the presence of high clouds. A similar result was found by Fueglistaler and Fu (2006), based on detailed radiative heating calculations at tropical locations. Our study quantifies these relationships in global reanalysis data sets, and highlights how convection and

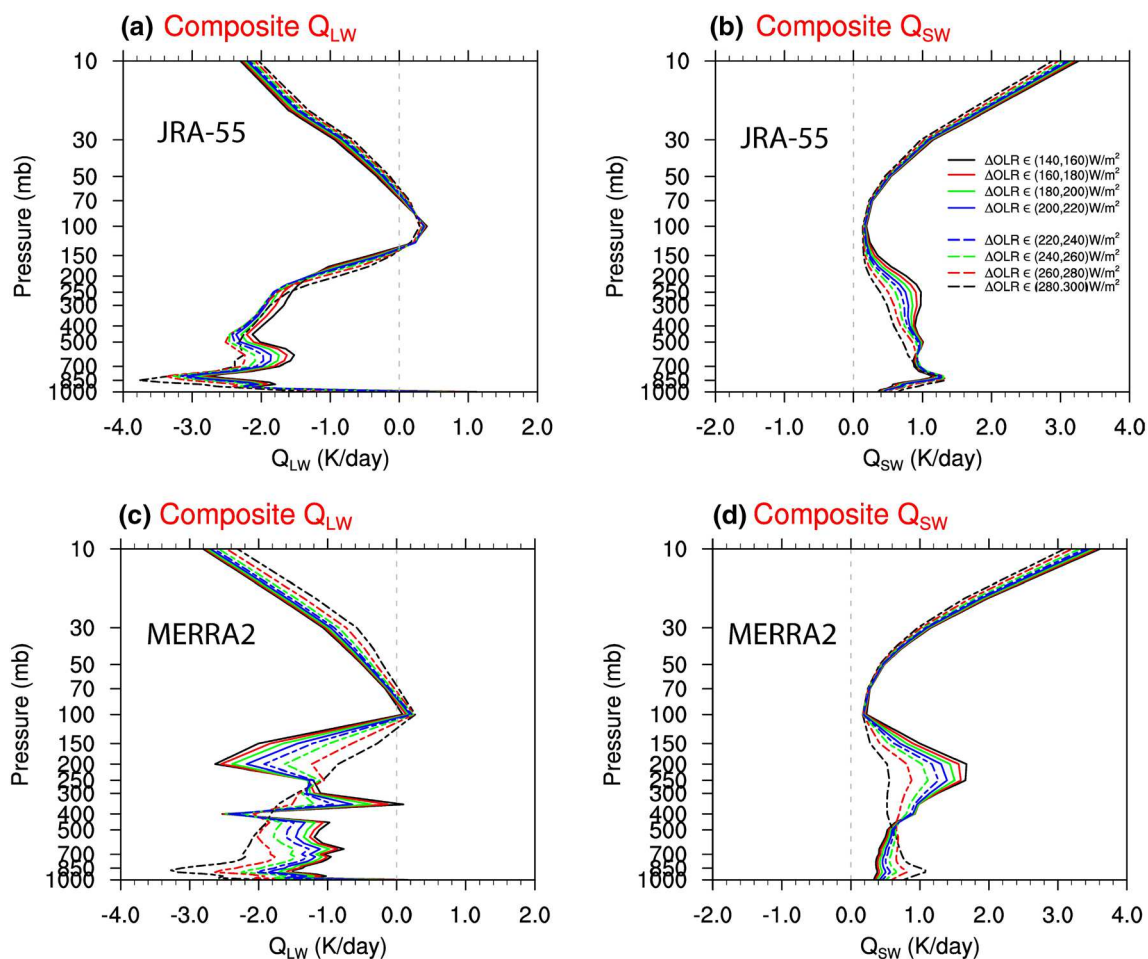


Fig. 16 Vertical profiles of Q_{LW} (left) and Q_{SW} (right) in the western Pacific, composited according to OLR values. Results are shown for JRA-55 (top) and MERRA2 (bottom). Corresponding results for ERA-Interim are shown in Fig. 10e, f

clouds systematically influence diabatic heat budgets in the stratosphere.

Convective influences on vertical profiles of the radiative heating rates in ERA-Interim diagnosed here are consistent with Yang et al. (2010), who calculate cloud radiative heating in the tropical UTLS within 30°N–S based on a detailed radiative transfer model along with observations of atmospheric composition and clouds (including thin cirrus). Their calculations indicate that the impact of clouds on net radiative heating has transitions from positive below 100 hPa to negative above 100 hPa, consistent with our Figs. 6b and 10c. They furthermore showed that the LW cloud influence is positive below ~165 hPa and negative above ~165 hPa, consistent with our Fig. 6d. In addition, our results show that the response of radiative heat in the extratropics is rather different, with net cooling in both upper troposphere and stratosphere due to enhanced convection.

The physical component in this study also includes the parameterized turbulent mixing, known as vertical diffusion

heating rates. While we have not isolated this term, it is generally about an order of magnitude smaller than the other components, although local variations can be as large as fluctuations of the radiative components (Flannaghan and Fueglistaler 2011). Because this is a highly parameterized and uncertain term in large-scale models, how it varies and responds to convection are still poorly understood.

Our analyses quantify systematic changes in Q_{LW} and Q_{SW} in the troposphere tied to deep convection, and comparisons with an idealized column radiation model suggest these variations are mainly a response to cloud fraction, water and ice content associated with deep convection. Results in the storm track are very similar among the reanalyses. However, in the tropics there are very large differences in analyzed cloud water and ice content (Fig. 17), and these are in turn reflected in substantial differences in (cloudy) radiative heating rates (Fig. 16). The discrepancies in the tropical UTLS among the reanalyses were also pointed out by Wright and Fueglistaler (2013). These large differences in analyzed tropical cloud

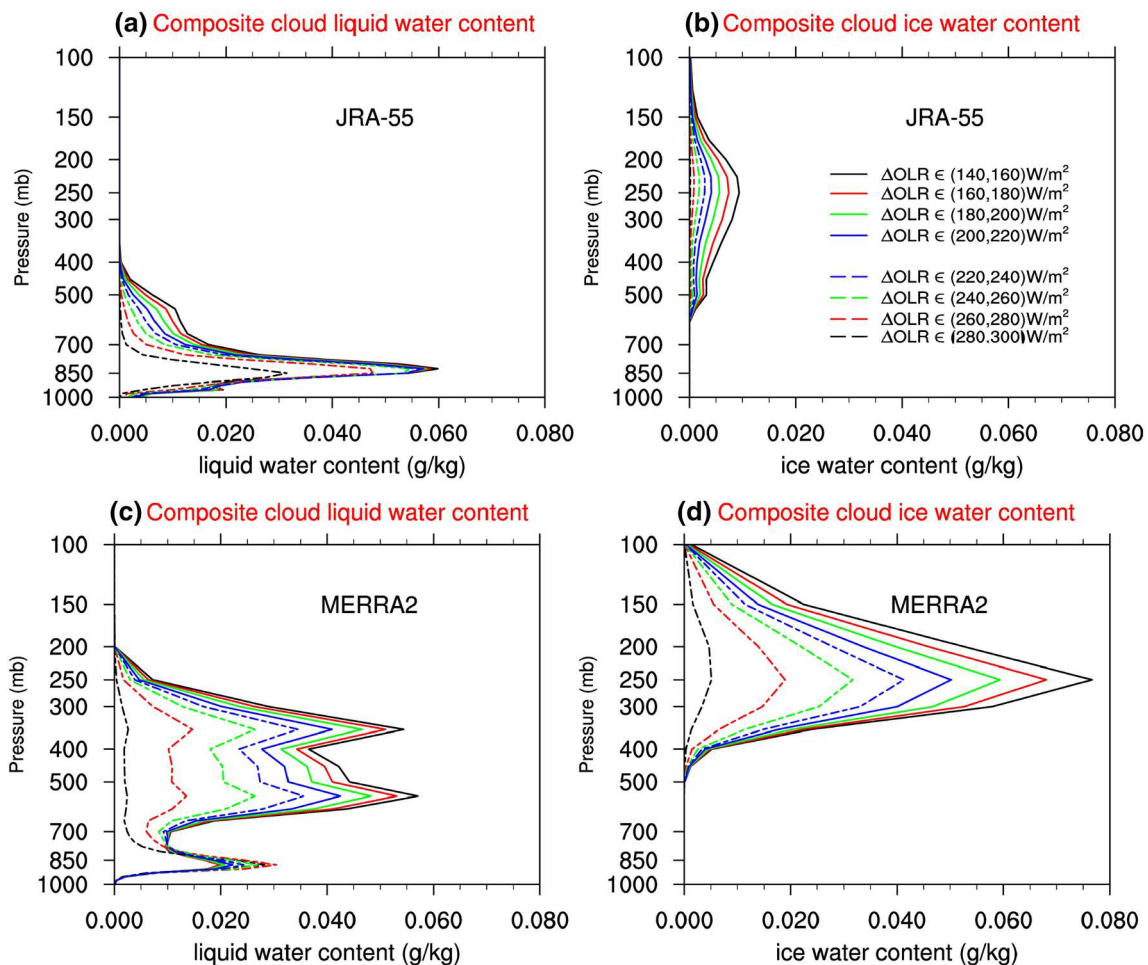


Fig. 17 Vertical profiles of cloud liquid water content (*left*) and cloud ice water content (*right*) in the western Pacific, composited according to OLR values. Results are shown for JRA-55 (*top*) and

MERRA2 (*bottom*). Note the very large differences between the reanalyses. Corresponding results for ERA-Interim are shown in Fig. 14c–e

behavior are a significant source of uncertainty in these current reanalyses.

Our calculations provide a simple statistical framework to evaluate variations in diabatic heating linked to transient deep convection in the climate system, such as MJO and monsoon systems. By looking at the changes of OLR, we can assess the temporal variations in diabatic heating profiles associated with convective fluctuations. The regimes of convection in the tropics have been shown to transit from shallow convection to midlevel congestus and then to deep convection (e.g., Johnson et al. 1999; Kikuchi and Takayabu 2004). Understanding how changes of diabatic heating are associated with these transitions is essential to study the development of various convective systems.

Acknowledgements We are grateful for useful discussions with Joowan Kim, Andrew Gettelman, and Thomas Birner, and thank an anonymous reviewer for constructive suggestions. The ERA-Interim diabatic heating datasets were retrieved via ECMWF Web API

(<https://software.ecmwf.int/wiki/display/WEBAPI/Access+ECMWF+Public+Datasets>). We thank Dr. Shaikh Mohammad, Peirong Lin and Dr. Chen Zhou for technical support. The RRTM code was downloaded from http://rtweb.aer.com/rtm_frame.html. This work was partially supported under the NASA Aura Science Team. The National Center for Atmospheric Research is operated by the University Corporation for Atmospheric Research, under sponsorship of the National Science Foundation.

References

- Bosilovich M, Lucchesi R, Suarez M (2015) MERRA-2: file specification. GMAO Office Note 9 (Version 1.0), p 73. https://gmao.gsfc.nasa.gov/pubs/office_notes/
- Bretherton CS (2007) Challenges in numerical modeling of tropical circulations, vol 3026330. Princeton University Press, Princeton
- Dee DP et al (2011) The ERA-Interim reanalysis: Configuration and performance of the data assimilation system. Q J R Meteorol Soc 137:553–597

- Flannaghan T, Fueglistaler S (2011) Kelvin waves and shear-flow turbulent mixing in the TTL in (re-) analysis data. *Geophys Res Lett* 38:L02801
- Fueglistaler S, Fu Q (2006) Impact of clouds on radiative heating rates in the tropical lower stratosphere. *J Geophys Res Atmos* 111:D23202
- Fueglistaler S, Legras B, Beljaars A, Morcrette JJ, Simmons A, Tompkins A, Uppala S (2009) The diabatic heat budget of the upper troposphere and lower/mid stratosphere in ECMWF reanalyses. *Q J R Meteorol Soc* 135:21–37
- Fung K, Ramaswamy V (1999) On shortwave radiation absorption in overcast atmospheres. *J Geophys Res: Atmos* 104:22233–22241
- Gottelman A et al (2004) Radiation balance of the tropical tropopause layer. *J Geophys Res Atmos* 109:D07103
- Gruber A, Krueger AF (1984) The status of the NOAA outgoing longwave radiation data set. *Bull Am Meteorol Soc* 65:958–962
- Gruber A, Winston JS (1978) Earth-atmosphere radiative heating based on NOAA scanning radiometer measurements. *Bull Am Meteorol Soc* 59:1570–1573
- Hartmann DL, Holton JR, Fu Q (2001) The heat balance of the tropical tropopause, cirrus, and stratospheric dehydration. *Geophys Res Lett* 28:1969–1972. doi:[10.1029/2000gl012833](https://doi.org/10.1029/2000gl012833)
- Hoskins BJ, Rodwell MJ (1995) A model of the Asian summer monsoon. Part I: the global scale. *J Atmos Sci* 52:1329–1340
- Houze RA (1989) Observed structure of mesoscale convective systems and implications for large-scale heating. *Q J R Meteorol Soc* 115:425–461
- Hu Y, Fu Q (2007) Observed poleward expansion of the Hadley circulation since 1979. *Atmos Chem Phys* 7:5229–5236
- Iacono MJ, Mlawer EJ, Clough SA, Morcrette J-J (2000) Impact of an improved longwave radiation model, RRTM, on the energy budget and thermodynamic properties of the NCAR community climate model, CCM3. *J Geophys Res* 105:14873–14890
- Johnson RH, Rickenbach TM, Rutledge SA, Ciesielski PE, Schubert WH (1999) Trimodal characteristics of tropical convection. *J Clim* 12(8):2397–2418
- Kikuchi K, Takayabu YN (2004) The development of organized convection associated with the MJO during TOGA COARE IOP: trimodal characteristics. *Geophys Res Lett* 31(10)
- Kobayashi S et al (2015) The JRA-55 reanalysis: general specifications and basic characteristics. *J Meteorol Soc Jpn* 93:5–48
- Li C, Jia X, Ling J, Zhou W, Zhang C (2009) Sensitivity of MJO simulations to diabatic heating profiles. *Clim Dyn* 32:167–187
- Liebmann B, Smith CA (1996) Description of a complete (interpolated) outgoing longwave radiation dataset. *Bull Am Meteorol Soc* 77:1275–1277
- Ling J, Zhang C (2013) Diabatic heating profiles in recent global reanalyses. *J Clim* 26:3307–3325
- Mlawer EJ, Taubman SJ, Brown PD, Iacono MJ, Clough SA (1997) Radiative transfer for inhomogeneous atmospheres: RRTM, a validated correlated-k model for the longwave. *J Geophys Res Atmos* 102:16663–16682
- Molod A, Takacs L, Suarez M, Bacmeister J (2015) Development of the GEOS-5 atmospheric general circulation model: evolution from MERRA to MERRA2. *Geosci Model Dev* 8:1339–1356
- Nigam S, Chung C, DeWeaver E (2000) ENSO diabatic heating in ECMWF and NCEP-NCAR reanalyses, and NCAR CCM3 simulation. *J Clim* 13:3152–3171
- Norton W (2001) Longwave heating of the tropical lower stratosphere. *Geophys Res Lett* 28:3653–3656
- Ohring G, Gruber A (1983) Satellite radiation observations and climate theory. *Adv Geophys* 25:237
- Ohring G, Gruber A, Ellingson R (1984) Satellite determinations of the relationship between total longwave radiation flux and infrared window radiance. *J Clim Appl Meteorol* 23(3):416–425
- Park M, Randel WJ, Gottelman A, Massie ST, Jiang JH (2007) Transport above the Asian summer monsoon anticyclone inferred from aura microwave limb sounder tracers. *J Geophys Res Atmos* 112:D16309
- Ploeger F, Konopka P, Günther G, Groöß JU, Müller R (2010) Impact of the vertical velocity scheme on modeling transport in the tropical tropopause layer. *J Geophys Res Atmos* 115:D03301
- Randel WJ, Zhang K, Fu R (2015) What controls stratospheric water vapor in the NH summer monsoon regions? *J Geophys Res Atmos* 120(15):7988–8001
- Rienecker MM et al (2011) MERRA: NASA's modern-era retrospective analysis for research and applications. *J Clim* 24:3624–3648
- Schoeberl MR, Dessler AE, Wang T (2012) Simulation of stratospheric water vapor and trends using three reanalyses. *Atmos Chem Phys* 12:6475–6487
- Schoeberl MR, Dessler A, Wang T (2013) Modeling upper tropospheric and lower stratospheric water vapor anomalies. *Atmos Chem Phys* 13:7783–7793
- Wang T, Randel WJ, Dessler AE, Schoeberl MR, Kinnison DE (2014) Trajectory model simulations of ozone (O₃) and carbon monoxide (CO) in the lower stratosphere. *Atmos Chem Phys* 14:7135–7147. doi:[10.5194/acp-14-7135-2014](https://doi.org/10.5194/acp-14-7135-2014)
- Wang T, Dessler AE, Schoeberl MR, Randel WJ, Kim JE (2015) The impact of temperature vertical structure on trajectory modeling of stratospheric water vapor. *Atmos Chem Phys* 15:3517–3526. doi:[10.5194/acp-15-3517-2015](https://doi.org/10.5194/acp-15-3517-2015)
- Wright J, Fueglistaler S (2013) Large differences in reanalyses of diabatic heating in the tropical upper troposphere and lower stratosphere. *Atmos Chem Phys* 13:9565–9576
- Xie P, Arkin PA (1998) Global monthly precipitation estimates from satellite-observed outgoing longwave radiation. *J Clim* 11:137–164
- Yang Q, Fu Q, Hu Y (2010) Radiative impacts of clouds in the tropical tropopause layer. *J Geophys Res Atmos* 115:D00H12
- Zhang K, Fu R, Wang T, Liu Y (2016) Impact of geographic variations of the convective and dehydration center on stratospheric water vapor over the Asian monsoon region. *Atmos Chem Phys* 16:7825–7835. doi:[10.5194/acp-16-7825-2016](https://doi.org/10.5194/acp-16-7825-2016)